

International Conference on Space Optics—ICSO 2022

Dubrovnik, Croatia

3–7 October 2022

Edited by Kyriaki Minoglou, Nikos Karafolas, and Bruno Cugny,



Stray light analysis of Compact Gas Imager



Stray light analysis of Compact Gas Imager

V. Khodnevych^a, D. Simeoni^a,

^aIRT Saint Exupéry, Garden Space, Building B, 240 Rue Evariste Galois, 06410, Biot, France

ABSTRACT

This paper presents a set of developed tools and methods for the stray light analysis of the Compact Gas Imager, a new sensor concept to capture images of gases, featuring a peculiar optical concept. The disruptive optical concept requires an adaptation of existing tools and the development of new technics for accurate stray light analysis. The described approach consists in deriving the stray light requirements from the requirements for the gas concentration by use of theoretical models and a set of approximations. The coupling of analytical models implemented in MatLab with conventional FRED modeling allows the assessment of stray light performance, i.e. the estimate of the impact of ghost (parasite interferograms) and diffuse stray light on the Compact Gas Imager performance. The analysis of the simulation results highlights the design changes and countermeasures required to achieve the system performance objectives.

The Compact Gas Imager concept associates interferometric and multispectral push broom imager technologies, thus the stray light methods and techniques discussed in the paper are suitable for a wide range of space applications.

Keywords: Compact Gas Imager, Stray light, Ghost analysis, scattering

1. INTRODUCTION

The Compact Gas Imager (CGI) is an optical instrument dedicated to the detection, quantification, and identification of gas sources in the atmosphere¹. Combining the advantages of an imager and a sounder, CGI delivers a high spatial resolution image of gases with high precision and accuracy measurements of gas concentration.

The relevant features of the spectral information are available for all scene points at once in the form of Partially Scanned Interferograms (PSI). A PSI is defined by a combination of spectral band, selected by bandpass filters, and optical path difference (OPD), generated by an interferometer. The selected OPD ranges correspond to a coherent rise caused by the periodicity of absorption rays of gases. The optimal choice of PSI definitions assures the highest sensitivity to the measured gases. Each PSI is the sum of a modulation and a baseline terms. The modulation results from the coherent sum of the beams of the two channels of the interferometer. The baseline results from the incoherent sum of two intensities from the two channels of the interferometer. The baseline information gives access to multispectral images. The Normalized Modulation Amplitude (NMA) of PSI (i.e. modulation amplitude divided by baseline) obtained for each pixel provides a good approximation (NMA hypothesis), for stray light analysis, of the gas concentration information¹.

A slight tilt between the two channels of the interferometer generates OPD in the image plane, creating interference fringes along the field of view of the detector. Figure 1 shows a simulation of one frame image acquired by CGI for the reference scene (Nuremberg) and uniform gas distribution in the NIR band. The absence of fringes at the top and bottom is caused by the shadow deadzone of the interferometer, i.e. zone in one channel of the interferometer, where the convergent beam is blocked by the difference in glass thickness.

The push-broom time delay integration principle is adapted to the acquisition of PSI: the image scrolling along the OPD axis, synchronized with the successive acquisition of frames, allows the acquisition of all PSI samples for all points of the scene.

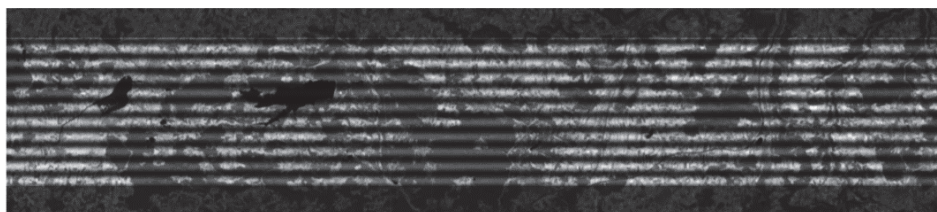


Figure 1. An illustrative frame image that is expected in CGI in the NIR band. The x and y directions are across and along the track directions of the detector.

The double nature of the instrument concept, multispectral imager, and static Fourier interferometer, defines combined requirements for precise radiometric measurements and high contrast imaging. Stray light (SL) affects both of them.

2. MODELS

2.1 Optical model

Figure 2 shows the optical model of CGI. The instrument is based on a static Fourier transform Michelson interferometer and it consists of four main parts: front optics (input objective), field widened static interferometer, back optics (Offner objective), and bandpass image filter.

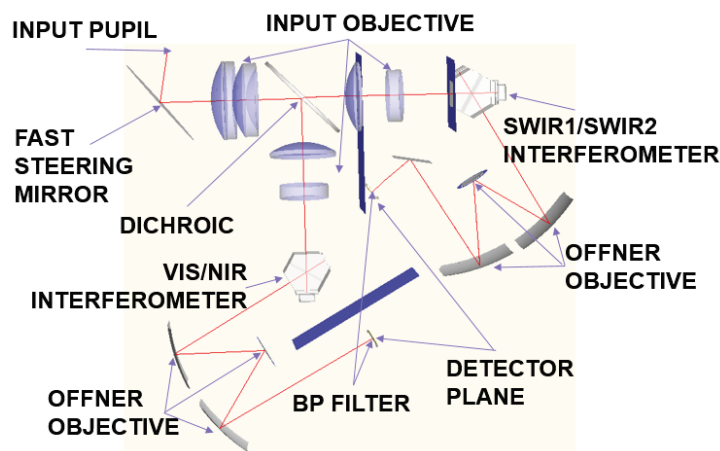


Figure 2 The optical design of CGI instrument in FRED. The structure of the instrument is ignored in the simulation, so a bunch of masks (dark blue planes) were set to cut unphysical paths. The red line is a chief ray.

The front optics creates an intermediate image on the mirrors of the interferometer. The interferometer accommodates several PSI with potentially different OPD. Except for constant OPD, mirror and glass surfaces have a small slope to introduce the difference of OPD along FoV. The interferometer, designed to be compact, polarization-insensitive, and achromatic, also features low SL contribution. The five-lenses Petzval front optics accommodates a dichroic after the 3rd lens. The dichroic divides VIS and NIR bands from SWIR1 and SWIR2 and so eases the optical design versus the chromatic requirements. The back optics is a three-mirror Offner telescope that relays the intermediate image plane of the interferometer to the detector plane. Telecentricity of objectives ensure appropriate illumination of the beam splitter coating and bandpass coatings. The bandpass spectral filter, placed in front of the detector, generates a set of spectral bands in the detector plane.

The optical design was done in CODEV and was manually imported in FRED for stray light analysis. The import verification was performed by comparison of RMS spot size in FRED and CODEV in five fields of view at the central

wavelength for each band. Besides this, irradiance verification with Lambertian source in the pupil plane was performed as well.

2.2 Stray light model

One of the biggest sources of errors in the SL analysis is a choice of the correct scattering model for optical and mechanical surfaces, so the choice was made with care. BSDF model parameters that were chosen for simulation are corresponding to typical values. In the study below we considered two sources of scattering: μ -roughness and contamination.

The model of μ -roughness is the Harvey-Shack model. As the modeled range of wavelengths is big (from the beginning of VIS up to SWIR2), correction on wavelength is required. For each band, three model coefficients were computed. The coefficients involve parameters of the fit of a measured surface roughness PSD with a typical RMS of 13.1 Å for optical surfaces². The same level of surface roughness is applied for each optical surface.

For scattering due to contamination, we are using the built-in FRED BRDF function based on the IEST CC1246D cleanliness standard. The model requires a few parameters, the most important of which is contamination level (CL). In the model, we assume that the optics of the interferometer will be in a sealed box and only the Fast steering mirror and first lens surface will be exposed to the space environment. For these two surfaces, we assume contamination of CL500 and for the rest CL300. Later on, the evolution of contamination and its effect on the measurement will be studied. In this preliminary study level of contamination is fixed. The slope of particle distribution is the same as in standard S=-0.926. The only changing parameter, except wavelength, is the refractive index of contamination. It is obtained from interpolation of the measured data³.

Each surface that interacts with light has an anti-reflection coating. The first ghost estimate is based on typical coating reflectances². The model consider two types of antireflection (AR) coating: moderate-performance AR coating (1% reflection) and high-performance AR coating (0.5% reflection). Surfaces close to the detector (backside of the filter substrate) or intermediate image plane (inside interferometer) are high-performance AR coated, the rest of the surfaces are moderate AR coated. All mirrors have 100% reflection. Interferometer edges and baffles have a black coating with 5% reflectivity. The bandpass filter is 5% reflecting in all the wavelengths and 95% transmission inside the band. Detector coating is 5% reflecting. Reflection coefficients are identical for all wavelengths.

Necessary for extensive scattering analyses, importance sampling is used. The essence of the importance sampling is the following: light scatters in all directions, but the only light that is reaching the detector surfaces is interesting for SL analysis, so discarding the scattering direction that cannot reach the detector, highly increases computational efficiency. In the current model, the importance sampling is set toward the next surface. To avoid computation errors, the importance sampling is not applied to the interferometer surfaces. For back optics, the forward and backward importance sampling takes into the Michelson interferometer reflection.

Analyses are carried out with the 3rd level of ancestry (ray splitting level) and the 1st level of scattering (scattering of scattered light is not considered); with Monte-Carlo ray splitting (at each interaction surface probabilistic power and direction for each ray are assigned) for non-uniform scene simulations (scattering and ghosts).

Model and analyses further development will consider scattering from coatings, realistic absorption of mechanical structure, edges, and bevels of lenses, baffling for out of nominal FoV SL, diffraction and, in fine, scratches and digs, volume scattering, molecular contaminations, micrometeoroid damage, and SL due to self-emission.

3. ANALYSIS OF UNIFORM SCENES

CGI delivers high spatial resolution images of gases with high precision and accuracy measurements of gas concentration. The goal of the section is to identify the impact of SL on radiometric performance.

3.1 SL radiometric bias error

The instrument requires precise radiometric measurements of baseline and modulation to achieve high accuracy in measurements of gas's concentration. Scattering due to particulate contamination and surface micro-roughness and ghosts lead to radiometric bias errors. A linear expansion of NMA gives access to a straightforward assessment of the effect of radiometric bias errors:

$$NMA^* = \frac{M+M^*}{B+O} \approx \frac{M}{B} \times \left(1 - \frac{O}{B} + \frac{M^*}{M}\right) \quad (1)$$

Where M, B are nominal modulation and baseline, and M^*, O are independent parasitic contributions for modulation (parasite ghost interference) and baseline (radiometric offset). Scattering causes offset of the baseline. Ghosts also contribute to offset of the baseline, but also to modulation parasitic contribution through a mechanism of interferences.

Parasite reflection from optical surfaces generates ghost beams. The overlap in the image plane of the ghost beam with one of the two nominal beams produces parasite interferograms. The here under formula expresses the spectral intensity per pixel taking into account spurious interferograms.

$$I(\sigma) = I_o(\sigma)(t_1 + t_2) + I_o(\sigma) \cdot 2\sqrt{t_1 t_2} \cdot C_{PSF} \cdot \cos(2\pi\sigma OPD) \\ + \sum_{Ghosts} t_G I_o(\sigma) + \sum I_o(\sigma) \cdot 2\sqrt{t_m t_l} \cdot C_{PSF_{m,l}} \cdot \cos(2\pi\sigma OPD_{m,l}) \quad (2)$$

t_1, t_2 are the transmission of the instrument for two nominal beams, t_G is the transmission of the ghost beam, and $I_o(\sigma)$ is the incoming spectral radiance. The radiance is the same for all beams, including the ghost beams. $OPD_{m,l}$ is the OPD between the ghost and the interfering nominal beams. SL generation of interferograms with OPD different from the optimal normally causes loss of modulation amplitude. C_{PSF} is the contrast of nominal beams interference. $C_{PSF_{m,l}}$ is the contrast of parasitic modulation. The difference between Point Spread Functions (PSF) and low PSF overlap induces a very low $C_{PSF_{m,l}}$ versus C_{PSF} ratio. The use of this simplistic approach allows the estimate of the contribution of ghosts to baseline offset.

$$\frac{O}{B} = \frac{\sum_{Ghosts} t_G}{t_1 + t_2} \quad (3)$$

3.2 Parasitic interferogram analysis

Optical simulation software such as FRED provides the estimate of the contribution of ghost to baseline offset (see Eq. 3), but not the assessment of the modulation contribution, which requires interferogram and contrast computation. This section describes the study of ghosts (without scattering), their ability to create parasite interferograms, and the impact of ghosts on the CGI measurements under the NMA hypothesis.

The first stage, with FRED stray light software, of the parasitic interferogram simulation identifies and analyses all significant ghosts. Ghost properties are partly FRED outputs and partly defined from the irradiance map of each ghost. The second stage, developed in MatLab, assesses performance from the list of ghosts with properties.

Ghost analysis is performed for each spectral band and five locations in FoV in the PSI zone. The simulation is performed in two scripted stages: ghost identification and ghost analysis. The ghost identification script finds all the ghost paths that satisfy certain criteria (transmission larger than $1e-5$ relative power and they reach detector surface). For each FoV, the ghost list is the same for simplicity. The filtered ghost paths are labeled as user-defined paths. The ghost analysis script carries out the analysis of the labeled ghosts one by one. The output of the analysis is an irradiance map, from which the RMS of the ghost (in X and Y direction) is computed and the power (transmission) of the ghost/nominal beam. The

irradiance map is analyzed in MatLab same as all associated values. OPD and OPD slope is computed in FRED. The OPD slope introduces OPD difference along-track of the detector and so a certain amount of fringes (typically 10). It is implemented by the surfaces with a slope in one of the interferometer channels. Multiple passages throw these surfaces cause accumulation of the OPD difference and so different amounts of fringes in the detector plane. The OPD slope is computed by counting the number of the intersection of the surfaces with the slope. The approximate method of contrast computation was used, due to the high aberration content of ghost beams. The contrast is estimated as:

$$C = \sqrt{\frac{RMS_x RMS_y}{rms_x rms_y}} \quad (4)$$

where in the numerator (RMS_x, RMS_y) is the size of the nominal beam and in the denominator is rms_x, rms_y of the ghost beam. Finally, for each FoV, the table of ghosts provides contrast, power (transmission), OPD, and OPD slope. The result of the FRED computation is a table with ghost list properties in the mat file. This file is used later in parasite interferogram computation. The calculation for the VIS/NIR channel of CGI identified 39 ghosts and 35 ghosts for SWIR1/SWIR2 channel.

The parasite interferogram computation model, implemented in MatLab and based on equation (2) is instantiated with the PSI definition (central wavelength, FWHM of the bandpass filter, number of samples, etc), file with ghost data (OPD, OPD slope, transmission, contrast), and top of atmosphere radiance spectrum file.

Only the interference of the ghost beam with the nominal beam is considered, as the other contributions are negligibly small. Each FoV script computes nominal (no SL) PSI and PSI with SL. Each PSI is analyzed under the NMA hypothesis. The output of the Matlab 1D PSI generator is Modulation, Baseline, and NMA for nominal paths and with SL (with ghosts). The fact that the modulation part of PSI is analyzed on modulation frequency only, numerically removes contribution from parasite interferogram that has another modulation frequency than the nominal one. The results of the analysis are summarized in table 1. The contribution of baseline and modulation is referring the NMA hypothesis (see equation 1).

The main contribution to NMA error is baseline offset (about 3.5%). The contribution of modulation is quite small because modulation is proportional to the interferometric contrast (see eq. 2) and the ghost's contrast is low due to high defocus. The most contributing are 1st order ghosts (parasite reflection between the intermediate image plane and detector). These are generated by all surfaces of the interferometer, bandpass filter substrate, and detector. But also the light that is reflected by the interferometer back to the input objective can contribute to ghosts (especially back surfaces of lenses L5 and L2). Ghost on the backside of the dichroic reflects SWIR light in the VIS/NIR channel, so good SWIR rejection is required or a SWIR insensitive detector.

Table 1 Mean contribution of baseline and modulation offset to radiometric bias error due to ghosts over FoV. The error corresponds to variations in FoV.

	VIS	NIR	SWIR1 CH4	SWIR1 CO2	SWIR2
O/B	0.037±0.005	0.034±0.005	0.034±0.006	0.033±0.005	0.037±0.002
M^*/M	3e-4±5e-4	2e-4±8e-4	0.008±0.006	0.004±0.009	0.003±0.006
$\Delta NMA/NMA$	0.0355	0.0328	0.0397	0.0277	0.0324

3.3 Discussion of the results

Table 2 gives contributors to the total content of power arriving on the detector. The scattering budget includes light that goes in the forward direction (from pupil to detector), and light that reflects from the interferometer and propagates to the entrance pupil (backscattering). One parasitic reflection ghosts (1st order) bring most of the SL power (about 3%). These "Michelson Interferometer" ghosts are one order of magnitude larger than "imager" two parasitic reflections Ghosts (2nd order) because of their high residual power. Scattering contribution increases for shorter wavelengths as expected.

Table 2. Stray light report for each spectral band. The percent distribution of total power arriving on the detector surface for a uniform scene simulation.

% of total power	VIS	NIR	SWIR1 CH4	SWIR1 CO2	SWIR2
Nominal beams	94,69	95,79	95,97	96,1	96,04
Ghost 1 st order	3,21	3,1	3,11	3,02	3,089
Ghost 2 nd order	0,43	0,4	0,4	0,4	0,41
Scattering	1,66	0,71	0,52	0,47	0,46
Total SL	5,31	4,21	4,03	3,9	3,96

The total SL ranges from 4% in SWIR bands, to 5% in VIS bands. The main SL contribution is through the baseline. The main SL contributor to radiometric bias error are the first-order ghosts. However, we stress the point that the bias can be corrected with calibration.

4. ANALYSIS OF NON-UNIFORM SCENES

Another complication of the radiometric bias errors is also the fact that SL pollutes also the neighboring pixels. This is well noticeable in the case of a high albedo gradient. Bright areas spread SL radiance on dark areas and can cause a large radiometric bias error in dark areas. This section shows the results of a quantitative estimate of this effect, from the simulation of non-uniform scenes.

The analysis of the straylight effect from non-uniform scenes is done with the same criteria as for CO2M mission⁴. At a 95% confidence level, the SL spectral radiance, outside the 500 m wide transition zone between bright and dark zones depicted in Figure 3, shall be smaller than 3% in NIR, SWIR1, SWIR2, and 5% in VIS. The spectral luminance of the light quadrant is twice as intense as the spectral luminance of the dark quadrant.

The non-uniform scene simulation consists of filtering, by the embedded script, the rays generated with a Lambertian source in the entrance pupil, i.e. Lambertian source generates rays in all directions, and the script traces the rays with the only angle of interest in accordance to the non-uniform scene. Figure 3 shows detector irradiance with SL in the SWIR2 band for a non-uniform scene.

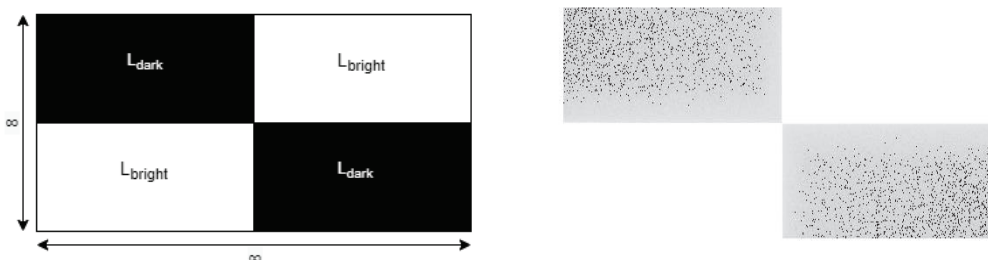


Figure 3. Non-uniform scene simulation, sketch on left is the same as in the CO2M requirement, figure on right is the result of FRED simulation in SWIR2 band of stray light propagation from illuminated quadrant to non-illuminated one.

The normalized difference between irradiance with SL and without SL (nominal path only) gives the SL contribution expressed in the percentage of SL.

$$\%SL = \frac{\langle E_{SL} \rangle - \langle E_{Nom} \rangle}{\langle E_{Nom} \rangle} \cdot 100\% \quad (5)$$

The error corresponds to a 95% confidence level. Table 3 shows that the level of SL slightly exceeds the requirements level. However, there are improvements envisioned that are promising option to reduce this straylight levels and come closer, if not to meet, the required performances. These enhancements are based on design changes and countermeasures:

design optimizations of interferometer and band filters including the implementation of high-performance rejection filters for ghost reduction, and less complex bandpass filters to minimize scattering.

Table 3 Amount of stray light in percent in dark and bright quadrants of the scene and mean over the uniform scene.

%	VIS	NIR	SWIR1 CH4	SWIR1 CO2	SWIR2
Dark	6.0±1.4	4.5±0.8	4.5±0.8	4.2±0.4	4.4±0.8
Bright	5.2±1.1	4±0.7	3.6±0.7	3.5±0.3	3.8±0.7
Mean	5.5±0.9	4.2±0.5	4.0±0.5	3.8±0.3	4±0.5

Further SL analysis refinement will include: the detailed design of all parts in the vicinity of optical beams, anodized or black coated structural parts than can increase scattering contribution, and detailed particulate contamination level based on assembly and sealing of interferometer and detection in a super clean environment (ISO3 or better). The detailed SL simulation will provide an SL Kernel for further SL corrections. Raw assessment of expected performance change with the listed above design and simulation improvements together with the SL characterization and numerical elimination at the frame image level gives a high degree of confidence that fine SL will achieve the measurement objective.

5. CONCLUSION

The development of a set of analytical and optical models and stray light analysis has enabled the identification and quantification of the impact of stray light on the high-level performance of the Compact Gas Imager concept.

The theoretical study has made it possible to express the contribution of spurious interferograms introduced by ghosts to the degradation of the CGI image performance. The exploitation of simulations done in FRED allowed the definition and quantification of SL contributors' origins: i.e. the physical place in the instrument and nature, i.e. the baseline or modulation of the interferograms. We showed that the main contributors to the CGI performance are baseline radiometric bias errors, and put in evidence that the modulation's contribution due to parasitic interferograms is much smaller. The highlight of all critical components that define SL performance allowed the identification of design improvements and SL characterization and calibration to in fine achieve the measurement objective of Compact Gas Imagers with detailed simulation. Stray light simulations of non-uniform scenes evidenced that the achievement of CO2M SL mission performance is realistic with Compact Gas Imager's enhanced design.

The here presented analysis is being refined with mechanical structure and detailed physical properties of coatings and filters. Besides this, the design upgrade will include input baffles to protect against sun and Earth out of the field of view fluxes and interferometer beam dumps and field stops to improve stray light rejection. Detailed interferometer design takes into account actual manufacturing constraints.

The methodology and tools presented here form a basis for stray light analysis that can be transposed to any other type of optical instrument combining highly accurate interferometric measurements and high-resolution imaging.

REFERENCES

- [1] Simeoni D. et al. "CarbonCGI road map to observe faint GHG source's emissions with high resolution observing system", SPIE Sensors, Berlin, (2022)
- [2] Fest E., "Stray light analysis and control", SPIE, (2013)
- [3] Jennings, S., Pinnick, R., Aubermann, H., "Effects of particulate complex refractive index and particle size distribution variations on atmospheric extinction and absorption for visible through middle IR wavelengths", Applied Optics, Vol. 17, pp. 3922-3929 (1978).
- [4] Copernicus High Priority Candidate Missions CO2M SSRD, CO2M-RS-ESA-SY-0002, issue 1, ESA, (2019)